Materials Science & Engineering A 563 (2013) 147–151

Contents lists available at SciVerse ScienceDirect

Materials Science & Engineering A

journal homepage: www.elsevier.com/locate/msea

The effect of silicon on the strengthening and work hardening of aluminum at room temperature

Qinglong Zhao *, Bjørn Holmedal

Department of Materials Science and Engineering, Norwegian University of Science and Technology, Trondheim N-7491, Norway

ARTICLE INFO

Article history:
Received 1 October 2012
Received in revised form
13 November 2012
Accepted 19 November 2012
Available online 27 November 2012

Keywords:
Aluminum alloys
Mechanical characterization
Mechanical properties
Portevin–Le Chatelier effect
Solid solution hardening

ABSTRACT

Solution hardening of Al–Si alloys at room temperature was investigated by tensile tests of several aluminum alloys containing various amounts of Si in solution but fabricated from the same commercially pure base material. It is found that Si has a weak strengthening effect but a significant impact on the work hardening. The strengthening was found to be very sensitive to water quenching, which enhances the solute strengthening. Despite the low strengthening effect, the Portevin–Le Chatelier effect was clearly observed during the tension of an alloy containing 0.4 at% Si, suggesting the occurrence of dynamic strain ageing due to surprisingly low levels of Si in solid solution.

1. Introduction

Non-heat-treatable aluminum alloys including AA1xxx (commercially pure aluminum), AA3xxx (Al–Mn) and AA5xxx (Al–Mg) systems are widely used in the applications requiring a low to medium strength, a good formability and a good corrosion resistance. Non-heat-treatable alloys owe their strength to the elements in solution, so solid solution hardening is an important strengthening mechanism in such alloys. Furthermore, the solute influence on the work hardening is important when it comes to formability. This is also the case for solution treated 6xxx alloys, where Si and Mg are the major elements in solution. In the commercial alloys a mix of elements are present in solid solution. The ultimate goal is to make models that can handle their complex interplay, and the natural starting point is the investigation of these elements one by one. Our understanding can be improved by atomistic simulations of atom core effects, such as those recently reported in [1,2].

The solute strengthening mechanism has been subjected to investigations for many years. The development of theories and many experimental results have been reviewed by several authors [3–5]. Mg and Mn have generally attracted more attention compared to other elements in aluminum, and studies on both high purity and commercial purity alloys have been reported [6,7]. Small amounts of Si usually exist in most commercial wrought aluminum alloys. Some of the Si atoms form constituent particles with Fe and also precipitate with other elements during heat treatments, while the remaining Si atoms are in solid solution. Hot deformation experiments of commercially pure Al–Si alloys [8] and theoretical calculations [1,2] indicate that Si has a weak solution hardening effect. However, few experimental results have been reported on cold deformation of aluminum containing various contents of Si in solution.

The Portevin–Le Chatelier (PLC) effect, which manifests itself as serrated flow and negative strain rate sensitivity, affects ductility and formability and has been extensively studied [9], especially in Al–Mg alloys. The PLC effect is associated with interaction of diffusing solute atoms with mobile dislocations, known as dynamic strain ageing (DSA). The PLC effect has been observed in Al–Si alloys containing 3–12 wt% Si at strain rates between 10^{-4} and $10^{-2}\,s^{-1}$ at room temperature [10,11]. In Ref. [11] the quenched-in vacancies were suggested to be the governing factor of PLC effect and the PLC effect was claimed to occur also in a Al–0.2 wt% Si binary alloy, but no results were shown for alloys with less than 3 wt% Si [11].

In this work, several aluminum alloys containing various amounts of Si in solution but fabricated from the same commercially pure base material, are investigated to explore the effect of Si on mechanical properties and the occurrence of PLC at room temperature.

2. Experimental

Aluminum alloys with three levels of Si contents were fabricated in the same manner by Hydro aluminum. The raw alloys are labeled

* Corresponding author. Tel.: +47 73596785; fax: +47 73550203.
E-mail address: qinglong.zhao@ntnu.no (Q.L. Zhao).

0921-5093/$ - see front matter © 2012 Elsevier B.V. All rights reserved.
http://dx.doi.org/10.1016/j.msea.2012.11.062

Table 1
The compositions and homogenization treatments.

Alloy	Al wt%	Nominal Si, wt%	Nominal Fe, wt%	Homogenization	Si in solution, at%
S1	99.73	0.07	0.15	833 K 6 h	0.03
S2	99.67	0.15	0.14	833 K 6 h	0.12
S5a	99.29	0.50	0.15	853 K 4 h +25 K/h to 673 K 4 h	0.34
S5b	99.29	0.50	0.15	833 K 6 h	0.43

as S1, S2 and S5 corresponding to the nominal content of Si (refer to Table 1). All the raw alloys were in the direct chill casting condition with a diameter of 22 cm. The S5 alloy was homogenized in two ways to achieve different levels of Si in solution, labeled as S5a and S5b, respectively. The compositions and homogenization treatments are listed in Table 1. Two sets of materials were prepared by different treatments following homogenization. One set of alloys was quenched into water after homogenization to induce excess vacancies. The other set was cooled in air to room temperature (cooling rate ~45 K/min) after homogenization to avoid inducing excess vacancies. The air cooled alloys were used to study solute strengthening of Al–Si, and the water quenched alloys were used to study the effect of quenching on solid solution hardening. All the materials were left at room temperature before further tests.

The solute concentrations in solid solution were measured by a JEOL JXA-8500F electron probe micro-analyzer (EPMA). The microstructure after homogenization was investigated by both a Zeiss Supra 55 field emission gun scanning electron microscope (FEG-SEM) operated at 15 kV and a JEOL 2010 transmission electron microscope (TEM) operated at 200 kV. The tensile tests were performed using cylindrical specimens with a diameter of 6 mm, a gauge length of 25 mm and a parallel length of 35 mm. Three parallel tests were performed for each alloy. An MTS 810 hydraulic testing machine was run under a constant ramp rate at room temperature, giving strain rates of about $10^{-1}\,s^{-1}$ and $10^{-3}\,s^{-1}$.

3. Results and discussion

3.1. Microstructure

The concentration of Fe in solid solution was about 0.01 at% (measured by EPMA), which in the present work is negligible. The atomic concentrations of Si in solid solution are listed in Table 1. Constituent particles are formed at dendrites and grain boundaries during casting and homogenization (Fig. 1). The constituent particles are expected to be mainly Fe_4Al_{13} and β-AlFeSi according to the ternary phase diagram [12], and in S5a some Si particles are formed during homogenization. The average radius of the constituent particles in all the alloys was ~0.7 μm, and the area fractions were ~0.3%. No fine precipitates were observed by TEM in the air cooled S5b, suggesting that no precipitation occurred during cooling. The texture is expected to be random due to the homogeneous cast structure. The grain sizes of the materials except S1 were similar, about 107 μm on average. S1 had coarser grains, and the mean diameter was 162 μm.

3.2. Portevin–Le Chatelier effect in Al–Si

The alloy with the highest amount of Si in solution (S5b) was tested by a strain rate change tensile test to illustrate the occurrence of the PLC effect in this alloy (Fig. 2). Both water quenched and air cooled S5b showed similar serrations in the tensile curves. Serrated yielding occurred at the strain rate of $10^{-3}\,s^{-1}$, showing type A serrations (Fig. 2). For a description of

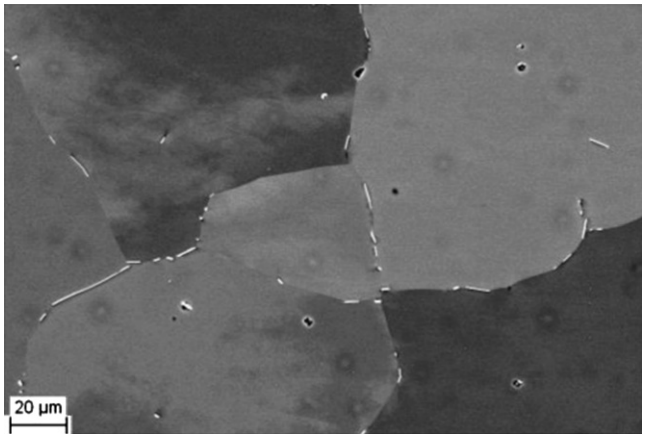

Fig. 1. Back-scattered electron image of constituent particles in S5b, showing that the coarse particles were distributed mainly at grain boundaries.

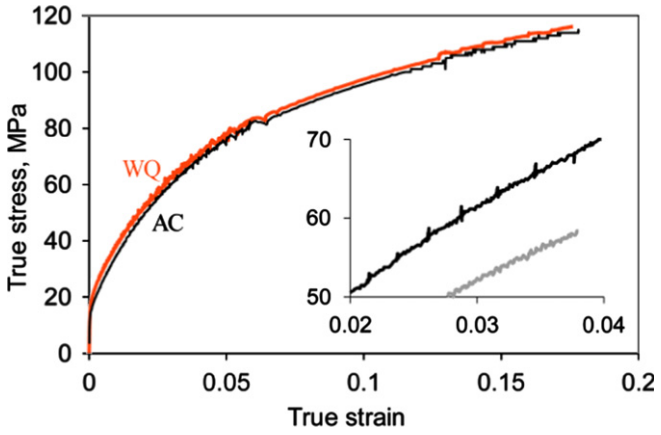

Fig. 2. Strain rate change during tensile test of water quenched (WQ) and air cooled (AC) S5b (initially $10^{-3}\,s^{-1}$, changed to $0.1\,s^{-1}$ at strain of 0.06, then back to $10^{-3}\,s^{-1}$ at strain of 0.13). The inserted figure illustrates the beginning of type A serrations with a gray line showing the fluctuations of a test on S1 (the line is shifted to appear in the same range as S5b).

the types of serrations, see Ref. [9]. A segment of the testing curve of S1 is also shown in Fig. 2, confirming that the type A serrations are clearly distinguishable from background fluctuations. The increase of the strain rate to $0.1\,s^{-1}$ at a strain of 0.06 reduced the serrated flow behavior in Fig. 2. However, serrated yielding reappeared (as type D) later at strains slightly larger than 0.1, still at the highest strain rate. However, the serrations became more pronounced when the strain rate was again changed back to $10^{-3}\,s^{-1}$ at a strain of 0.13. Type A serrations were also observed in S5a, but less pronounced. The presence of the PLC effect confirms that DSA occurs in a dilute Al–Si alloy, and furthermore that the quenched-in excess vacancies in the water quenched specimen did not affect the PLC effect.

In general DSA is expected in Al–Si alloys, since Si has similar diffusion coefficient as Mg in aluminum [13]. The PLC effect has also earlier been observed in supersaturated Al–Si alloys [10,11]. Early research on Al–1 wt% Si alloy wires and ribbons [14] noted that the tensile curves were serrated at room temperature regardless of the quenching rate; whereas the tensile curves tested at 197 K were smooth. This observation indicates that the PLC effect is due to DSA. The PLC effect in a dilute Al–Si alloy is demonstrated in Fig. 2. The occurrence of PLC requires the concentration to be larger than a certain critical value. The critical concentration for Al–Mg at room temperature has been estimated to be 0.86 wt%, and accordingly the PLC effect was not observed in a

Al–0.45 wt% Mg [15]. On the other hand the Al–0.43 at% Si alloy (S5b) in this work shows the PLC effect, indicating that Si results in a stronger DSA than Mg. Curtin et al. [16] demonstrated the cross-core model of DSA for Al–Mg to be mono-atom-hop motion of solutes from the compression to the tension side of the edge dislocation core. A similar mechanism may also be applicable to explain how the DSA occurs in dilute Al–Si alloys. The size misfit of Si in an aluminum matrix is about half of Mg and is of opposite sign [2], hence the atomic jump will be in the opposite direction across the core. The dislocation interactions with solutes Si can be investigated by atomistic simulations and might be different than with Mg.

3.3. The mechanical properties of Al–Si alloys

True stress–strain curves from tensile tests at a strain rate of $\sim 0.1\ s^{-1}$ are shown in Fig. 3. The flow stresses were almost similar at the initial stage of plastic deformation, but the influence of Si on the flow stress became more significant as the strain increased. The addition of Si increased the ultimate tensile strength (UTS) but decreased the uniform elongation as shown in Table 2.

The yield strength of the alloys was increased by water quenching compared to the air cooled alloys (Fig. 3b), implying that quenched-in vacancies somehow contributed to the strength. However, the stress–strain curves of the water quenched alloy and the air cooled converged at larger strains, so the UTS and uniform elongation were not affected by quenching (Table 2). It suggests that the effect of quenching is restricted to a short transient subsequent to yielding, and quenching does not affect the further work hardening.

3.4. Solid solution hardening

Generally the flow stress is affected by the solute content, particles and the grain size. The constituent particles in the present alloys were relatively large and of a small volume fraction and formed at dendrite and grain boundaries. They affect the flow stress to a limited amount. The contribution to the flow stress of the grain size is estimated by the Hall–Petch relation, where a Hall–Petch parameter, k in $kd^{-1/2}$ of $k=0.78\ \mathrm{MPa\ mm^{1/2}}$ for 99.5% commercially pure aluminum [17] is used for the calculations. According to these calculations, the difference in yield stress between S1 and the other materials due to the grain size contribution is found to be $\sim$0.4 MPa. This small contribution of grain size to the flow stress is negligible and comparable to the experimental errors. The relation between the flow stress and the solute concentration is commonly expressed as

$$\sigma = \sigma_0 + Hc^n, \quad (1)$$

where σ_0 is the flow stress of the pure metal, and H and n are constants. All the materials investigated in this work may be classified as commercially pure aluminum alloys. The value of H at strain of 0.002 indicates the solute effect on the yield strength, while at higher strains H reflects the combination of the solute effect on strength and work hardening. Eq. (1) can be used to estimate the solution hardening of Si for a comparison with literature works. The exponent n in general is in the range from 0.5 to 1, and its precise value has been found to be close to 1 for Al–Mg alloys. The value of H in Eq. (1) for Mg is $\sim$14.3 MPa/at% in both commercially pure [6] and high-purity aluminum [7] with $n=1$. For the considered Al–Si alloys, the value of H in Eq. (1) for air cooled Al–Si is determined to be 7.6 MPa/at% and σ_0 is 16.2 MPa, using $n=1$. The strengthening effect of Si is thus nearly half that of Mg in aluminum at room temperature. The value of H for the water quenched Al–Si alloys is determined to be 12.6 MPa/at% (with $\sigma_0=19.6$ MPa). If quench hardening is independent of solid solution hardening, the value of H would not be affected by the quenching. The difference in the values of H between the air cooled alloys and the water quenched ones suggests that the strengthening effect of quenching is enhanced by the solutes, implying that solutes interact with quenched-in vacancies.

The flow stress of the air cooled and water quenched Al–Si alloys in this work and Al–Mg alloys from Ref. [6] at various strains is plotted as a function of the atomic concentration of solutes in Fig. 4. The Al–Mg alloys in Ref. [6] had similar contents of Si and Fe as S1 in this work. Linear trend lines of Al–Mg are also plotted in Fig. 4. It should be noted that the Al–Mg alloys [6] were tested at a strain rate of $\sim 10^{-3}\ s^{-1}$. It has been reported that the yield strength of Al–Mg alloys is affected weakly by strain rates below $10\ s^{-1}$, and that the yield strength at the strain rate of $0.1\ s^{-1}$ was no stronger than those at lower strain rates [7]. Hence, the different strain rates should not affect much the comparison of Al–Si and Al–Mg. The 0.2% yield stresses of air cooled Al–Si are below the linear trend line of Al–Mg (the dashed line in Fig. 4), suggesting that the influence of Si on solution hardening is weaker than of Mg. However, the flow stresses of

Table 2
Ultimate tensile strength (UTS) and uniform elongation (UE) of air cooled and water quenched Al–Si alloys.

Alloy	Air cooled		Water quenched	
	UTS, MPa	UE,%	UTS, MPa	UE,%
S1	75.7	35	75.3	34
S2	81.5	33	81.7	33
S5a	94.5	29	94.8	29
S5b	98.6	29	99.4	28

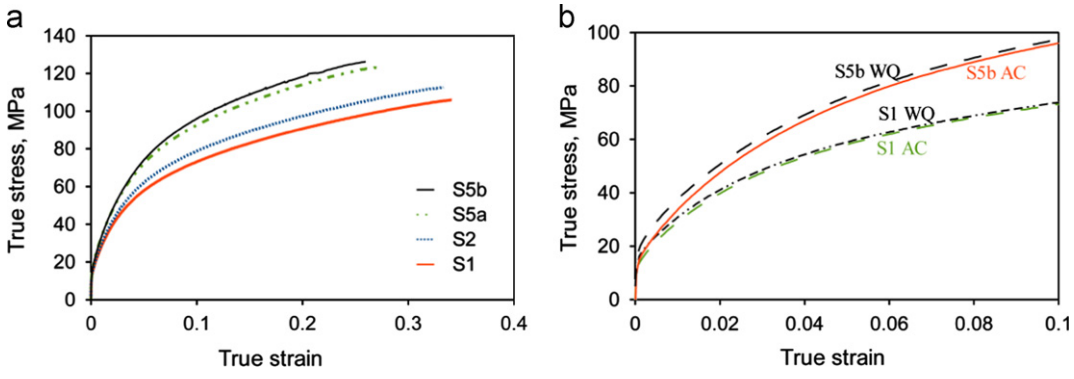

Fig. 3. (a) Stress–strain curves of air cooled Al–Si alloys from tensile tests at a strain rate of $\sim 0.1\ s^{-1}$. (b) Comparison of stress–strain curves of air cooled (AC) and water quenched (WQ) alloys in the initial part of the stress–strain curves.

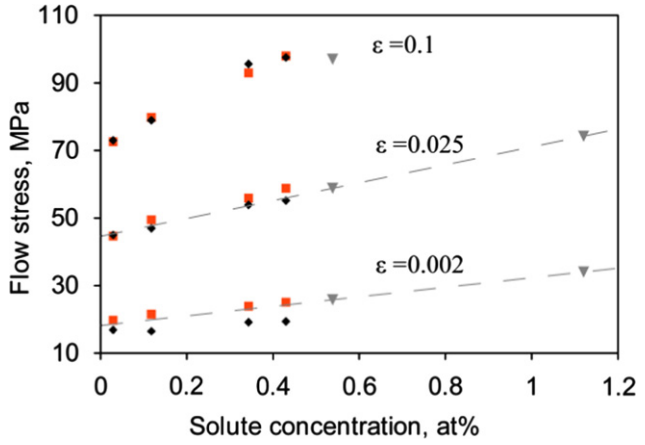

Fig. 4. Flow stress as a function of solute concentration at various strains. ■, water quenched Al–Si alloys; ♦, air cooled Al–Si alloys; ∇, Al–Mg alloys from Ref. [6], and linear trend lines are included for Al–Mg (dashed lines).

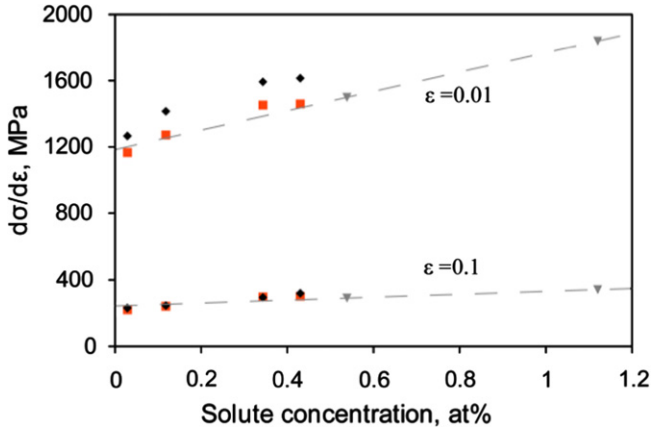

Fig. 5. Work hardening rates as a function of solute concentrations at various strains, suggesting that solutes increase work hardening rates. ■, water quenched Al–Si alloys; ♦, air cooled Al–Si alloys; ∇, Al–Mg alloys from Ref. [6], including linear trend lines for Al–Mg.

Al–Si fit well with the same trend line of Al–Mg at a strain of 0.025, suggesting that the flow stress of Al–Si is no lower than Al–Mg at larger strains. This indicates that Si has a stronger effect than Mg on the work hardening. The comparison between water quenched and air cooled alloys in Fig. 4 confirms that the quench hardening contribution vanishes as the strain increases.

The solid solution hardening arises due to the strain fields from the solute atoms in the matrix, and the strain field is related to the size misfit and modulus misfit. The size and modulus misfits of Si are about half of the values of Mg [18], so the hardening effect of Si has been theoretically predicted using first-principles atomistic calculations to be much weaker than Mg, less than half of that of Mg at low temperatures [2]. The concentration dependence of solute strengthening can be estimated from the classical theories (Labusch or Friedel). At higher temperatures, the temperature dependence has to be considered. The energy barrier of Si for dislocations is predicted to be smaller than that of Mg [2], suggesting that the decrease of the hardening effect of Si with increasing temperature is more rapid than that of Mg. Thus, the solution hardening of Si atoms in theory should be much weaker than that of Mg atoms at room temperature. The stress contribution by solution hardening, $\Delta\sigma_s$ at elevated temperatures can be calculated from the model in Ref. [2]. The values of $\Delta\sigma_s$ at 290 K are calculated to be 2.2 MPa for S5a, and 2.8 MPa for S5b. The experimental differences between the yield strength and σ_0 in Eq. (1) are 3.0 MPa for S5a, and 3.2 MPa for S5b. The model predictions are thus in good agreement with the measurements.

3.5. Work hardening

The work hardening rates $d\sigma/d\varepsilon$ at strains of 0.01 and 0.1 of Al–Si and Al–Mg [6] are plotted in Fig. 5a. The values of work hardening rates of Al–Si at a strain of 0.01 are above the trend line for Al–Mg, suggesting that Si has a stronger effect than Mg on the work hardening. As a consequence the Al–Si and the Al–Mg strengths are very similar at a strain of 0.025 in Fig. 4, although the initial strength of Al–Si was much weaker than Al–Mg. Also at a strain of 0.1 the effect of Si on work hardening remains similar as for Al–Mg.

Work hardening is a result of dislocation storage and their dynamic recovery. The strain rate does not affect evidently the athermal storage of dislocations, but affects dynamic recovery significantly [19,20]. The tensile tests of Al–Mg at various strain rates in [21] indicates that DSA enhances the work hardening by a lower dynamic recovery at small strain rates. A possible explanation for this is suggested based on a simplistic picture of dynamic recovery events occurring as annihilations of dipole configurations [19], where opposite dipole segments have to move a distance equal to the dipole spacing in order to annihilate. Their movement would in general also involve cross slip or climb, which might be differently influenced by the Si solutes than the glide of mobile dislocations. The energy barrier of the dipole segment movement decreases with the decreased dipole spacing. Thus, the velocity of the dipole segment increases with the decreased dipole spacing. At early stage of deformation, the average dipole spacing is large due to low dislocation density. The velocity of the dipole segment might be sufficiently small that the dipole movement is subject to DSA, i.e. it is more effectively dragged by solute atoms than the glide of mobile dislocations. Thus, a strong DSA effect weakens the dynamic recovery and increases the work hardening. It explains the initial increased work hardening rate in Al–Si as compared to Al–Mg [6] by the stronger DSA effect of Si in aluminum. As strain increases, the average dipole spacing decreases due to the increased dislocation density. Hence such segments move with an increased speed so that the DSA effect is not effective. At larger strains ($\geqq\sim 0.1$), the dependency of work hardening on the solute level is similar for Al–Si as for Al–Mn and Al–Mg [6].

4. Summary

Si in aluminum has a weak strengthening effect at room temperature, but increases the work hardening significantly at strains below 0.1. Quenching increases the yield strength of Al–Si alloys, but its effect diminishes as strain increases and does not affect the flow stress and work hardening at strains larger than 0.1. The dependency of strengthening on the solute level in water quenched Al–Si alloys is stronger than that in air cooled alloys, implying that Si solutes interact with quenched-in vacancies. It requires further investigations to clarify the mechanism of such interactions. The occurrence of PLC in a dilute Al–Si alloy is confirmed in the present work. Quenching does not affect the PLC effect. It is suggested that DSA retards the dynamic recovery at small strains, causing an enhanced initial work hardening. DSA involves dislocation core interactions between dislocation segments and Si atoms that may be studied by atomistic

simulations similar as those for Al–Mg alloys [16]. An improved understanding of such reactions is important in order to model the strength and work hardening of Al–Si alloys and ultimately of industrial multi-component solid solution alloys.

Acknowledgment

This work is funded by Research Council of Norway, Hydro and Sapa under the project MOREAL.

References

[1] G.P.M. Leyson, W.A. Curtin, L.G. Hector, C.F. Woodward, Nat. Mater. 9 (2010) 750–755.
[2] G.P.M. Leyson, L.G. Hector Jr., W.A. Curtin, Acta Mater. 60 (2012) 3873–3884.
[3] P. Haasen, Solution hardening in FCC metals, in: F.R.N. Nabarro (Ed.), Dislocations in Solids, North-Holland, New York, 1979, pp. 155–189.
[4] P. Haasen, Mechanical properties of solid solutions, in: R.W. Cahn, P. Haasen (Eds.), Physical Metallurgy, 4th edition,North-Holland, Oxford, 1996, pp. 2009–2073.
[5] H. Neuhäuser, C. Schwink, Solid solution strengthening, in: R.W. Cahn, P. Haasen, E.J. Kramer (Eds.), Materials Science and Technology: A Comprehensive Treatment, Wiley-VCH, Weinheim, 2005.
[6] Ø. Ryen, O. Nijs, E. Sjölander, B. Holmedal, H.E. Ekström, E. Nes, Metall. Mater. Trans. A 37 (2006) 1999–2006.
[7] T. Mukai, K. Higashi, S. Tanimura, Mater. Sci. Eng., A 176 (1994) 181–189.
[8] B. Rønning, K. Nord-Varhaug, T. Furu, E. Nes, Mater. Sci. Forum 331 (2000) 571–576.
[9] J.M. Robinson, M.P. Shaw, Int. Mater. Rev 39 (1994) 113–122.
[10] G. Rajaram, S. Kumaran, S. Suwas, Mater. Sci. Eng., A 528 (2011) 6271–6278.
[11] M. Niinomi, T. Kobayashi, K. Ikeda, J. Mater. Sci. Lett. 5 (1986) 847–848.
[12] G. Ghosh, Al–Fe–Si (Aluminium–Iron–Silicon), in: G. Effenberg, S. Ilyenko (Eds.,) Light Metal Ternary Systems: Phase Diagrams, Crystallographic and Thermodynamic Data, SpringerMaterials – The Landolt-Börnstein Database, 2008.
[13] Y. Du, Y.A. Chang, B. Huang, W. Gong, Z. Jin, H. Xu, Z. Yuan, Y. Liu, Y. He, F.Y. Xie, Mater. Sci. Eng., A 363 (2003) 140–151.
[14] H.S. Rosenbaum, D. Turnbull, Acta Metall. 6 (1958) 653–659.
[15] N.Q. Chinh, F. Csikor, Z. Kovacs, J. Lendvai, J. Mater. Res. 15 (2000) 1037–1040.
[16] W. Curtin, D. Olmsted, L. Hector, Nat. Mater. 5 (2006) 875–880.
[17] N. Hansen, Acta Metall. 25 (1977) 863–869.
[18] J. Zander, R. Sandström, L. Vitos, Comput. Mater. Sci. 41 (2007) 86–95.
[19] E. Nes, K. Marthinsen, Y. Brechet, Scr. Mater. 47 (2002) 607–611.
[20] U.F. Kocks, H. Mecking, Prog. Mater. Sci. 48 (2003) 171–273.
[21] O.-G. Lademo, O. Engler, A. Benallal, O.S. Hopperstad, Int. J. Mater. Res 103 (2012) 1035–1041.